PDE Traffic Observer Validated on Freeway Data

Huan Yu[ID], Qijian Gan, Alexandre Bayen, *Member, IEEE*,
and Miroslav Krstic[ID], *Fellow, IEEE*

Abstract— This article develops a boundary observer for the estimation of congested freeway traffic states based on the Aw–Rascle–Zhang (ARZ) partial differential equations (PDEs) model. Traffic state estimation refers to the acquisition of traffic state information from partially observed traffic data. This problem is relevant for freeway due to its limited accessibility to real-time traffic information. We propose a model-driven approach in which the estimation of aggregated traffic states in a freeway segment is obtained simply from the boundary measurement of flow and velocity without knowledge of the initial states. The macroscopic traffic dynamics is represented by the ARZ model, a 2 × 2 coupled nonlinear hyperbolic PDEs for traffic density and velocity. Using the PDE backstepping method, we construct a boundary observer consisting of a copy of the nonlinear plant with output injections from boundary measurement errors. The exponential stability of the estimation error system in the L^2 norm and finite-time convergence to zero is guaranteed. Numerical simulation and data validation are conducted to validate the boundary observer design with vehicle trajectory data.

Index Terms— Aw–Rascle–Zhang model, backstepping method, boundary observer, data validation, traffic estimation.

I. INTRODUCTION

TRAFFIC state estimation plays an important role in traffic management. In order to mitigate freeway traffic congestion, various control algorithms [5], [20], [26], [32], [33], [37], [38] are developed for ramp metering or variable speed limit. However, their performance heavily relies on accurate measurement of traffic states on mainline freeways. Due to financial and technical limitations, it is difficult to measure traffic states on mainline freeways everywhere at all times. Therefore, it is important to estimate traffic states at places where detection is missing.

The topic of traffic state estimation refers to foreseeing traffic states with partially observed traffic data and some prior knowledge of traffic. Such a topic has been extensively studied and attracted a lot of attention in recent decades. According to the comprehensive review in [29], approaches on

traffic estimation fall into the following three categories: model driven, data driven, and streaming data driven. Among them, the model-driven approach is the most popular one and has been widely used to solve various traffic estimation problems. Compared with the data-driven approach, the model-based approach provides an accurate estimation with less input data and is also easier to identify the reason even if the estimation is inaccurate or the model is not the representative of the traffic data. The model-based estimation can be integrated with traffic control operations directly. The disadvantage of this approach is that it requires careful selection and calibration of the model. As a first step in the model-driven approach, traffic flow models are often used to describe traffic dynamics and are calibrated with historical data. Then, state estimates are obtained based on the calibrated model and real-time data inputs. Therefore, it is crucial for traffic estimation to have an advanced physical model that describes freeway traffic dynamics accurately. This motivates us to employ the state-of-the-art second-order traffic partial differential equation (PDE) model for traffic state estimation.

Freeway traffic dynamics in spatial and temporal domains are usually described using macroscopic models with aggregated variables of traffic density, velocity, and flux. These aggregated variables average out small-scale noises of freeway traffic and can be directly measured by stationary/point-based sensors, such as loop detectors. Among the macroscopic models, the Lighthill–Whitham–Richards (LWR) model in [23] and [28] is one of the most applied models. This model is a first-order scalar hyperbolic PDE of density and can predict the propagation and dissipation of traffic shockwaves and represent the fundamental phenomena of free and congested regime of traffic. Several studies in [6]–[8] and [22] have used such a model for traffic states' estimation due to its simplicity and efficiency in model calibration and numerical simulation. However, the LWR model fails to describe stop-and-go traffic, which is the oscillatory behavior of congested traffic. The main reason is because the static equilibrium density–velocity relation of the LWR model is unable to reproduce the nonequilibrium relation appearing in the stop-and-go traffic.

In order to address this limitation, second-order models are proposed to employ a nonlinear hyperbolic PDE for traffic velocity, in addition to the density conservation equation. Therefore, deviations from the equilibrium traffic relation are allowed in the second-order model since the dynamics of the velocity PDE is captured. The first well-known second-order model is the Payne–Whitham (PW) model in [27] and [30].

However, it predicts negative traffic velocity that is physically unrealistic. Later in [3] and [36], the Aw–Rascle–Zhang (ARZ) model was proposed, which successfully addresses the anisotropic behavior of traffic and corrects the PW model's prediction of traffic waves. For this reason, the ARZ model has been studied intensively for the stop-and-go traffic over the recent years [4], [16], [17], [21].

There have been many studies applying second-order traffic models as physical models for state estimation, for example, the second-order extended cell-transmission model in [25] and the second-order PW model in [31]. Kalman filter extensions and variations are used in [25] and [31] to estimate the most probable state that allows observation to correct the model's prediction. The data assimilation approach based on the Kalman filter extensions and variations allows observation to correct the model's prediction. The model and the measurement are not regarded as perfect. Instead, the approach estimates the most probable state. However, the noise may raise the need for additional calibration, which generally requires larger amounts of data. The observer model is developed for the spatially discretized traffic flow model whose accuracy depends on the discretization and the numerical schemes to be used and may require more complicated model calibration. However, to the best of our knowledge, the state-of-the-art ARZ PDE model has never been used for state estimation. In order to accurately estimate the nonequilibrium traffic states for congested traffic, this article employs the second-order ARZ PDE model. A boundary observer is designed for the PDE model using the backstepping method and is validated with traffic field data. Compared with the data assimilation approach, the observer proposed in this article requires less measurement information, easier model calibration, and works directly with the original second-order PDE model instead of the discretized one.

In dealing with the second-order coupled nonlinear hyperbolic system, PDE control of the ARZ model has been studied through many recent efforts [4], [18], [20], [32], [33], and [37]. The previous work by Yu and Krstic [32], [33] first adopts the PDE backstepping methodology for control of the ARZ model. Boundary control and observer design using the PDE backstepping method have been developed for 2×2 coupled hyperbolic systems [11] and for the general heterodirectional hyperbolic systems in [1], [12], and [24]. The applications of the theoretical results include open-channel flow, oil drilling, heat exchangers, and multiphase flow problems but have never been considered in traffic problems.

In [32], an observer design is proposed for the linearized ARZ model in an effort to construct an output feedback controller. In [35], we generalize the previous observer design to address the freeway traffic estimation problem from a more practical perspective. In specific, the observer design is implemented for the nonlinear ARZ model with certain assumptions of boundary conditions being removed. The observer design accepts a general functional form of the equilibrium density–velocity relation rather than a basic choice of Greenshield's model so that the PDE model has a better data fitting in calibration. Data validation results in this article are obtained based on the theoretical result in [35].

In validation of the observer, vehicle trajectory data are used to obtain the aggregated values of traffic states. The ARZ model is calibrated with the field data. The model parameters are mostly obtained from the historical data. The rest is determined from part of the data set. Then, the observer is constructed using the model parameters and real-time sensing of the data at boundaries. The performance of the PDE boundary observer is then evaluated with the field data of the temporal and spatial domains.

The contribution of this article is as follows. A systematic model-driven approach is developed for traffic state estimation. The PDE boundary observer based on the macroscopic ARZ traffic model is designed and validated. The theoretical observer design by a backstepping method is generalized and adapted for the field-data validation. Vehicle trajectories data [15] are used to construct and test the performance of the observer design. This result paves the way for implementing the PDE observer design in practice and gives rise to a variety of opportunities to incorporate the PDE backstepping techniques in solving a freeway traffic estimation problem.

The outline of this article is as follows. In Section II, we first introduce the nonlinear ARZ model and analyze the linearized ARZ model for distinguishing the free and congested traffic. Section III designs the boundary observer for the linearized ARZ model using the backstepping method and the nonlinear boundary observer is developed using the output injections obtained from the linearized model. In Section IV, numerical simulation of the nonlinear ARZ PDE model and state estimation by nonlinear implementation of the boundary observer is conducted first from an *ad hoc* choice of model parameters. In Section V, we calibrate the ARZ model with some field data and test the observer's performance. The estimation errors are then analyzed.

II. Problem Statement

We consider the traffic estimation problem for a stretch of freeway whose length is L. The macroscopic traffic dynamics is described by the ARZ model. We study the linearized ARZ model and discuss the characteristic speeds under free and congested traffic regime.

A. Aw–Rascle–Zhang Model

The ARZ model for $(x, t) \in [0, L] \times [0, +\infty)$ is given

$$\partial_t \rho + \partial_x (\rho v) = 0 \tag{1}$$

$$\partial_t v + \left(v - \rho p'(\rho)\right)\partial_x v = \frac{V(\rho) - v}{\tau}. \tag{2}$$

The state variable $\rho(x, t)$ denotes the traffic density and $v(x, t)$ denotes the traffic speed. The equilibrium velocity–density relationship $V(\rho)$ is a decreasing function of density. The equilibrium flux function $Q(\rho)$, also known as fundamental diagram, is defined as

$$Q(\rho) = \rho V(\rho). \tag{3}$$

For the ARZ model, the velocity functional form $V(\rho)$ needs to be chosen such that it is strictly decreasing $V'(\rho) < 0$ and the flux function $Q(\rho)$ is smooth, strictly concave $Q(\rho)'' < 0$.

The second-order ARZ model is valid when the hyperbolicity is ensured for $Q(\rho)$. One of the basic choice of $V(\rho)$ is in the form of Greenshield's model

$$V(\rho) = v_f \left(1 - \left(\frac{\rho}{\rho_m}\right)^\gamma\right) \tag{4}$$

where ρ_m is the maximum density and v_f is the maximum velocity. The observer design proposed in Section III is not limited by this choice. Later on, a more realistic functional form of $V(\rho)$ is employed to obtain a better fitting with the traffic field data.

The inhomogeneous ARZ model includes a relaxation term on the right-hand side of the velocity PDE. The constant parameter τ is the relaxation time, which describes drivers' driving behavior adapting to equilibrium density–velocity relation over time. Note that the homogeneous ARZ model without the relaxation term cannot address this phenomenon and also poses as an easier estimation problem.

The increasing function of density $p(\rho)$ is defined as the traffic pressure

$$p(\rho) = C_0 \rho^\gamma \tag{5}$$

where $C_0, \gamma \in \mathbb{R}_+$, $p'(\rho) > 0$, and $p(0) = 0$ are assumed. The pressure function $p(\rho)$ is chosen to relate the equilibrium velocity–density function $V(\rho)$ by the following:

$$p(\rho) = V(0) - V(\rho). \tag{6}$$

Given $V(\rho)$ in (4), we have density pressure as

$$p(\rho) = v_f \left(\frac{\rho}{\rho_m}\right)^\gamma. \tag{7}$$

Note that the abovementioned relations lead to a marginal linear stability [32]. It can be physically interpreted as a very slow damping effect of the stop-and-go traffic. The following boundary observer design can be easily adapted if the relation (6) does not hold.

B. Linearized ARZ Model in Traffic Flux and Velocity

The traffic density is defined as the number of vehicles per unit length. The traffic flux represents the number of vehicles per unit time crossing a fixed point on the road. The traffic flow flux q is defined as

$$q = \rho v. \tag{8}$$

Traffic flux q and velocity v are the most accessible physical variables to measure in freeway traffic. q is commonly measured by loop detectors and v can be obtained by GPS or high-speed cameras. Therefore, we rewrite the ARZ model in traffic flux q and traffic velocity v as follows,

$$\partial_t q + v \partial_x q = \frac{q}{v}\left(v + \frac{q}{v}V'\left(\frac{q}{v}\right)\right)\partial_x v + \frac{Q\left(\frac{q}{v}\right) - q}{\tau} \tag{9}$$

$$\partial_t v + \left(v + \frac{q}{v}V'\left(\frac{q}{v}\right)\right)\partial_x v = \frac{V\left(\frac{q}{v}\right) - v}{\tau}. \tag{10}$$

There is no explicit solution to the abovementioned nonlinear coupled hyperbolic system. To further understand the dynamics of the ARZ traffic model in the (q, v)-system, we linearize the model around steady states $(q^\star, v^\star)$ that are chosen as spatial and temporal nominal values of state variables. Small deviations from the nominal profile are defined as

$$\tilde{q}(x, t) = q(x, t) - q^\star \tag{11}$$

$$\tilde{v}(x, t) = v(x, t) - v^\star. \tag{12}$$

The steady density is given as $\rho^\star = q^\star/v^\star$. The set point density–velocity relation satisfies the equilibrium relation $V(\rho)$

$$v^\star = V(\rho^\star). \tag{13}$$

The linearized ARZ model in $(\tilde{q}, \tilde{v})$ around the reference system $(q^\star, v^\star)$ with boundary conditions is given by

$$\partial_t \tilde{q} + \lambda_1 \partial_x \tilde{q} = -\frac{q^\star}{v^\star}\left(v^\star + \frac{q^\star}{v^\star}V'\left(\frac{q^\star}{v^\star}\right)\right)\partial_x \tilde{v}$$
$$- q^\star \frac{(v^\star)^2 + q^\star V'\left(\frac{q^\star}{v^\star}\right)}{\tau(v^\star)^3}\tilde{v} + \frac{q^\star V'\left(\frac{q^\star}{v^\star}\right)}{\tau(v^\star)^2}\tilde{q} \tag{14}$$

$$\partial_t \tilde{v} + \lambda_2 \partial_x \tilde{v} = -\frac{(v^\star)^2 + q^\star V'\left(\frac{q^\star}{v^\star}\right)}{\tau(v^\star)^2}\tilde{v} + \frac{V'\left(\frac{q^\star}{v^\star}\right)}{\tau v^\star}\tilde{q} \tag{15}$$

where the two characteristic speeds of the abovementioned linearized PDE model are

$$\lambda_1 = v^\star \tag{16}$$

$$\lambda_2 = v^\star + \frac{q^\star}{v^\star}V'\left(\frac{q^\star}{v^\star}\right). \tag{17}$$

1) *Free-Flow Regime $(\lambda_1 > 0, \ \lambda_2 > 0)$:*
   In the free-flow regime, both the disturbances of traffic flux and velocity travel downstream, at respective characteristic speeds λ_1 and λ_2. The linearized ARZ model in a free regime is a homo-directional hyperbolic system.

2) *Congested Regime $(\lambda_1 > 0, \ \lambda_2 < 0)$:*
   In the congested regime, the traffic density is greater than the critical value ρ_c that satisfies $Q(\rho)'|_{\rho_c} = 0$ and the second characteristic speed λ_2 becomes the negative value. Therefore, the disturbances of the traffic speed travel upstream with λ_2, whereas the disturbances of the traffic flow flux are carried downstream with the characteristic speed λ_1. The hetero-directional propagations of disturbances force vehicles into the stop-and-go driving.

In the free-flow regime, the linearized homodirectional hyperbolic PDEs can be solved explicitly by the inlet boundary values, and therefore, state estimates are obtained by solving the linearized hyperbolic PDEs directly. In this article, we focus on the congested regime with two heterodirectional hyperbolic PDEs. It is a more relevant and challenging problem for traffic states' estimation.

III. BOUNDARY OBSERVER DESIGN

In this section, boundary sensing is employed for the observer design. The state estimation of the nonlinear ARZ model is achieved using the backstepping method. The output

injection gains are designed for the linearized ARZ model and then are added to a copy of the nonlinear plant.

Boundary values of state variations from the steady states are defined as

$$Y_{q,\text{in}}(t) = \tilde{q}(0, t) \tag{18}$$

$$Y_{q,\text{out}}(t) = \tilde{q}(L, t) \tag{19}$$

$$Y_v(t) = \tilde{v}(L, t) \tag{20}$$

where the values of $\tilde{q}(0, t)$, $\tilde{q}(L, t)$, and $\tilde{v}(L, t)$ are obtained by subtracting set point values $(q^\star, v^\star)$ from the sensing of incoming traffic flux $q(0, t)$, outgoing flux $q(L, t)$, and outgoing velocity $v(L, t)$, according to (11) and (12). In practice, sensing of the aggregated values of the traffic flux and velocity

$$y_q(t) = q(0, t) \tag{21}$$

$$y_{\text{out}}(t) = q(L, t) \tag{22}$$

$$y_v(t) = v(L, t) \tag{23}$$

is usually obtained by high-speed cameras or induction loop detectors. The induction loops are coils of wire embedded in the surface of road to detect the changes of inductance caused by passage of vehicles. The high-speed cameras record the vehicle trajectories for a freeway segment.

A. Output Injection for the Linearized ARZ Model

We diagonalize the linearized equations and therefore write $(\tilde{q}, \tilde{v})$-system in the Riemann coordinates. The Riemann variables are defined as

$$\xi_1 = \frac{\rho^\star \lambda_2}{\lambda_1 - \lambda_2} \tilde{v} + \tilde{q} \tag{24}$$

$$\xi_2 = \frac{q^\star}{\lambda_1 - \lambda_2} \tilde{v}. \tag{25}$$

The inverse transformation is given by

$$\tilde{v} = \frac{\lambda_1 - \lambda_2}{q^\star} \xi_2 \tag{26}$$

$$\tilde{q} = \xi_1 - \frac{\lambda_2}{\lambda_1} \xi_2. \tag{27}$$

The measurements are taken at boundaries, and we evaluate (26) and (27) at boundaries, which leads to the following boundary conditions:

$$\xi_1(0, t) = \frac{\lambda_2}{\lambda_1} \xi_2(0, t) + Y_{q,\text{in}}(t) \tag{28}$$

$$\xi_2(L, t) = \frac{q^\star}{\lambda_1 - \lambda_2} Y_v(t). \tag{29}$$

Therefore, the linearized ARZ model in the Riemann coordinates is obtained

$$\partial_t \xi_1 + \lambda_1 \partial_x \xi_1 = -\frac{1}{\tau} \xi_1 \tag{30}$$

$$\partial_t \xi_2 + \lambda_2 \partial_x \xi_2 = -\frac{1}{\tau} \xi_1 \tag{31}$$

$$\xi_1(0, t) = \frac{\lambda_2}{\lambda_1} \xi_2(0, t) + Y_{q,\text{in}}(t) \tag{32}$$

$$\xi_2(L, t) = \xi_1(L, t). \tag{33}$$

In order to diagonalize the right-hand side to implement the backstepping method, we introduce a scaled state as follows:

$$\bar{w}(x, t) = \exp\left(\frac{x}{\tau \lambda_1}\right) \xi_1(x, t) \tag{34}$$

$$\bar{v}(x, t) = \xi_2(x, t). \tag{35}$$

The (ξ_1, ξ_2)-system is then transformed to a first-order 2×2 hyperbolic system

$$\partial_t \bar{w}(x, t) + \lambda_1 \partial_x \bar{w}(x, t) = 0 \tag{36}$$

$$\partial_t \bar{v}(x, t) + \lambda_2 \partial_x \bar{v}(x, t) = c(x) \bar{w}(x, t) \tag{37}$$

$$\bar{w}(0, t) = \frac{\lambda_2}{\lambda_1} \bar{v}(0, t) + Y_{q,\text{in}}(t) \tag{38}$$

$$\bar{v}(L, t) = \frac{q^\star}{\lambda_1 - \lambda_2} Y_v(t) \tag{39}$$

where the spatially varying parameter $c(x)$ is defined as

$$c(x) = -\frac{1}{\tau} \exp\left(-\frac{x}{\tau \lambda_1}\right). \tag{40}$$

Parameter $c(x)$ is a strictly increasing function and bounded by

$$-\frac{1}{\tau} \leq c(x) \leq -\frac{1}{\tau} \exp\left(-\frac{L}{\tau \lambda_1}\right). \tag{41}$$

Then, we design a boundary observer for the linearized ARZ model to estimate $\bar{w}(x, t)$ and $\bar{v}(x, t)$ by constructing the following system:

$$\partial_t \hat{w}(x, t) + \lambda_1 \partial_x \hat{w}(x, t) = r(x)(\bar{w}(L, t) - \hat{w}(L, t)) \tag{42}$$

$$\partial_t \hat{v}(x, t) + \lambda_2 \partial_x \hat{v}(x, t) = c(x) \hat{w}(x, t)$$
$$+ s(x)(\bar{w}(L, t) - \hat{w}(L, t)) \tag{43}$$

$$\hat{w}(0, t) = \frac{\lambda_2}{\lambda_1} \hat{v}(0, t) + Y_{q,\text{in}}(t), \tag{44}$$

$$\hat{v}(L, t) = \frac{q^\star}{\lambda_1 - \lambda_2} Y_v(t) \tag{45}$$

where $\hat{w}(x, t)$ and $\hat{v}(x, t)$ are the estimates of the state variables $\bar{w}(x, t)$ and $\bar{v}(x, t)$, respectively. The value $\bar{w}(L, t)$ is obtained from (24) and (34) evaluated at $x = L$. We have $\xi_1(L, t) = (\rho^\star \lambda_2)/(\lambda_1 - \lambda_2) \tilde{v}(L, t) + \tilde{q}(L, t)$. Substituting the measurements $Y_v(t) = \tilde{v}(L, t)$ and $Y_{q,\text{out}}(t) = \tilde{q}(L, t)$, we obtain the following measurement of $\bar{w}(L, t)$:

$$\bar{w}(L, t) = \exp\left(\frac{L}{\tau \lambda_1}\right)\left(\frac{\rho^\star \lambda_2}{\lambda_1 - \lambda_2} Y_v(t) + Y_{q,\text{out}}(t)\right). \tag{46}$$

The terms $r(x)$ and $s(x)$ are output injection gains to be designed. We denote estimation errors as

$$\check{w}(x, t) = \bar{w}(x, t) - \hat{w}(x, t) \tag{47}$$

$$\check{v}(x, t) = \bar{v}(x, t) - \hat{v}(x, t). \tag{48}$$

The error system is obtained by subtracting the estimates (42)–(45) from (36)–(39)

$$\partial_t \check{w}(x, t) + \lambda_1 \partial_x \check{w}(x, t) = r(x) \check{w}(L, t) \tag{49}$$

$$\partial_t \check{v}(x, t) + \lambda_2 \partial_x \check{v}(x, t) = c(x) \check{w}(x, t) + s(x) \check{w}(L, t) \tag{50}$$

$$\check{w}(0, t) = \frac{\lambda_2}{\lambda_1} \check{v}(0, t) \tag{51}$$

$$\check{v}(L, t) = 0. \tag{52}$$

The design of output injection gains $r(x)$ and $s(x)$ needs to guarantee that the error system $(\check{w}, \check{v})$ decays to zero. Using the backstepping transformation, we transform the error system (49)–(52) into the following target system:

$$\partial_t \alpha(x, t) + \lambda_1 \partial_x \alpha(x, t) = 0 \tag{53}$$

$$\partial_t \beta(x, t) + \lambda_2 \partial_x \beta(x, t) = 0 \tag{54}$$

$$\alpha(0, t) = \frac{\lambda_2}{\lambda_1} \beta(0, t) \tag{55}$$

$$\beta(L, t) = 0. \tag{56}$$

The explicit solution to the target system (53)–(56) is easily found

$$\alpha(x, t) = \alpha\left(0, t - \frac{x}{\lambda_1}\right), \qquad t > \frac{L}{|\lambda_1|} \tag{57}$$

$$\beta(x, t) = \beta\left(L, t + \frac{L - x}{\lambda_2}\right), \quad t > \frac{L}{|\lambda_2|}. \tag{58}$$

Thus, we have

$$\alpha(x, t) \equiv \beta(x, t) \equiv 0 \tag{59}$$

after a finite time $t = t_f$, where

$$t_f = \frac{L}{|\lambda_1|} + \frac{L}{|\lambda_2|}. \tag{60}$$

It is straightforward to prove that the (α, β)-system is exponentially stable in the L^2 sense.

The backstepping transformation is given in the form of spatial Volterra integral

$$\alpha(x, t) = \check{w}(x, t) - \int_x^L K(L + x - \xi)\check{w}(\xi, t)d\xi \tag{61}$$

$$\beta(x, t) = \check{v}(x, t) - \int_x^L M(\lambda_1 x - \lambda_2 \xi)\check{w}(\xi, t)d\xi \tag{62}$$

where the kernel variables $K(x)$ and $M(x)$ map the error system into the target system where the coupling term on the right-hand side is eliminated by the output injections. The kernel $M(x)$ is defined as

$$M(x) = -\frac{1}{\lambda_1 - \lambda_2} c\left(\frac{x}{\lambda_1 - \lambda_2}\right). \tag{63}$$

For boundary condition (55) to hold, the kernels $K(x)$ and $M(x)$ satisfy the following relation:

$$K(L - \xi) = M((\lambda_2 - \lambda_1)\xi). \tag{64}$$

The kernel K is then obtained

$$K(x) = -\frac{1}{\lambda_1 - \lambda_2} c\left(\frac{-\lambda_2}{\lambda_1 - \lambda_2}(L - x)\right). \tag{65}$$

According to the boundedness of $c(x)$ in (41), the kernels are bounded by

$$|K(x)| \le \frac{1}{(\lambda_1 - \lambda_2)\tau} \tag{66}$$

and therefore, $M(x)$ is bounded. The output injection gains $r(x)$ and $s(x)$ are given by

$$r(x) = \lambda_1 K(x) = -\frac{\lambda_1}{\lambda_1 - \lambda_2} c\left(-\frac{\lambda_2}{\lambda_1 - \lambda_2}(L - x)\right) \tag{67}$$

$$s(x) = -\lambda_1 M(\lambda_1 x - \lambda_2 L)$$

$$= \frac{\lambda_1}{\lambda_1 - \lambda_2} c\left(x - \frac{\lambda_2}{\lambda_1 - \lambda_2}(L - x)\right) \tag{68}$$

such that the transformed target system (53)–(56) converges to zero. The backstepping transformation (61) and (62) is invertible. Therefore, we obtain the stability of the error system through the target system (53)–(56). We arrive at the following theorem.

Theorem 1: Consider system (49)–(52) with initial conditions $\check{w}_0, \check{v}_0 \in L^2([0, L])$. The equilibrium $\check{w} \equiv \check{v} \equiv 0$ is exponentially stable in the L^2 sense. It holds that

$$||\bar{w}(\cdot, t) - \hat{w}(\cdot, t)|| \to 0 \tag{69}$$

$$||\bar{v}(\cdot, t) - \hat{v}(\cdot, t)|| \to 0 \tag{70}$$

and the convergence to the equilibrium is reached in the finite time $t = t_f$ given in (60).

B. Nonlinear Implementation of the Observer Design

For nonlinear implementation of the observer design, we construct the system by keeping the output injections that are designed for the linearized ARZ model and then add them to a copy of the original nonlinear ARZ model.

We summarize the transformation from the linearized ARZ model in the $(\tilde{q}, \tilde{v})$-system to $(\bar{w}, \bar{v})$-system

$$\bar{w}(x, t) = \exp\left(\frac{x}{\tau \lambda_1}\right)\left(\frac{\rho^\star \lambda_2}{\lambda_1 - \lambda_2}\tilde{v}(x, t) + \tilde{q}(x, t)\right) \tag{71}$$

$$\bar{v}(x, t) = \frac{q^\star}{\lambda_1 - \lambda_2}\tilde{v}(x, t). \tag{72}$$

Also, the inverse transformation is given by

$$\tilde{q}(x, t) = \exp\left(-\frac{x}{\tau \lambda_1}\right)\bar{w}(x, t) - \frac{\lambda_2}{\lambda_1}\bar{v}(x, t) \tag{73}$$

$$\tilde{v}(x, t) = \frac{\lambda_1 - \lambda_2}{q^\star}\bar{v}(\xi, t). \tag{74}$$

The same transformation holds between the estimates $(\hat{w}, \hat{v})$ of the transformed states $(\bar{w}, \bar{v})$ and the state estimates $(\check{q}, \check{v})$ of $(\tilde{q}, \tilde{v})$-system. Due to the equivalence between $(\bar{w}, \bar{v}, \hat{w}, \hat{v})$ and $(\tilde{q}, \tilde{v}, \check{q}, \check{v})$-system, we arrive at the following theorem for the linearized ARZ model according to the stability property (69) and (70) in Theorem 1. The estimation errors of the linearized system are denoted by $\acute{q} = \tilde{q} - \check{q}, \acute{v} = \tilde{v} - \check{v}$.

Theorem 2: Consider the estimated system with initial conditions $\acute{q}_0, \acute{v}_0 \in L^2([0, L])$. The equilibrium $\acute{q} \equiv \acute{v} \equiv 0$ is exponentially stable in the L^2 sense. It holds that

$$||\tilde{q}(\cdot, t) - \check{q}(\cdot, t)|| \to 0 \tag{75}$$

$$||\tilde{v}(\cdot, t) - \check{v}(\cdot, t)|| \to 0 \tag{76}$$

and the convergence to zero is reached in the finite time $t = t_f$.

We denote the error injections designed for the linearized ARZ model (42)–(45) as

$$E_w(t) = r(x)(\bar{w}(L, t) - \hat{w}(L, t)) \tag{77}$$

$$E_v(t) = s(x)(\bar{w}(L, t) - \hat{w}(L, t)). \tag{78}$$

The output injection gains $r(x)$ and $s(x)$ are designed in (67) and (68). According to (46), $\bar{w}(L, t)$ is obtained from the real-time measurement of the traffic boundary data in (18)–(20). Therefore, the values of output injections $E_w(t)$ and $E_v(t)$ are known.

TABLE I

PARAMETER TABLE

Parameter Name	Value
Maximum traffic density ρ_m	160 vehicles/km
Traffic pressure coefficient γ	1
Maximum traffic velocity v_f	40 m/s
Relaxation time τ	60 s
Reference density $\rho^\star$	120 vehicles/km
Reference velocity $v^\star$	10 m/s
Freeway segment length L	500 m

The nonlinear implementation of the observer for state estimation of density and velocity $(\hat{\rho}(x,t), \hat{v}(x,t))$ is obtained by combining the copy of the nonlinear ARZ model (ρ, v) given by (1) and (2) and the abovementioned linear injection errors in the original state variables density and velocity

$$\partial_t \hat{\rho} + \partial_x(\hat{\rho}\hat{v}) = \frac{1}{v^\star}\left(\exp\left(-\frac{L}{\tau\lambda_1}\right)E_w - E_v\right) \quad (79)$$

$$\partial_t \hat{v} + (\hat{v} + \hat{\rho}V'(\hat{\rho}))\partial_x\hat{v} = \frac{V(\hat{\rho}) - \hat{v}}{\tau} + \frac{\lambda_1 - \lambda_2}{q^\star}E_v \quad (80)$$

where the linear injections on the right-hand side are obtained from (73), (74), (77), and (78). The boundary conditions are

$$\hat{\rho}(0,t) = \frac{y_q(t)}{\hat{v}(0,t)} \quad (81)$$

$$\hat{v}(L,t) = y_v(t). \quad (82)$$

The boundary measurement of the incoming traffic flux $y_q(t)$ and the outgoing velocity $y_v(t)$ is used in the abovementioned boundary conditions of the proposed observer. The boundary measurement of the outgoing traffic flux $y_{out}(t)$ and the outgoing velocity $y_v(t)$ appears in the output error injection terms (77) and (78) and, thus, in the observer equations (79) and (80). The output injection terms drive the observer to converge to the original nonlinear ARZ model. When the initial states of the system is close to the equilibrium, the linearized part dominates the nonlinear estimation error system. Therefore, the L^2 exponential stability and the finite-time convergence are achieved for the linearized ARZ model. In [11], the local exponential stability in H^2 sense is obtained for a quasi-linear hyperbolic PDE system with backstepping full-state feedback controller. The nonlinear ARZ model belongs to the class of the hyperbolic system discussed in [11]. The duality of the proposed observer design in (79)–(82) to the stabilization problem in [11] would yield a local H^2 stability result for the estimation problem, following the Lyapunov proof of Theorem 4.1 in [11]. Since we mainly focus on the practical implementation of the observer, we do not pursue a theoretical proof of the local analysis of the error system. Compared with the linearized observer design, this observer yields a better estimation result due to the fact that it induces less errors brought in by the model linearization. In Sections IV and V, the estimation result is first validated in numerical simulation with an *ad hoc* choice of model parameters and initial conditions and then validated with the traffic field data.

IV. NUMERICAL SIMULATION

For simulation of the nonlinear ARZ PDE model, we assume that the initial conditions are sinusoidal oscillations around the steady states $(\rho^\star, v^\star)$ that are in the congested regime. The initial conditions are assumed to be

$$\rho(x,0) = 0.1\sin\left(\frac{3\pi x}{L}\right)\rho^\star + \rho^\star \quad (83)$$

$$v(x,0) = -0.1\sin\left(\frac{3\pi x}{L}\right)v^\star + v^\star. \quad (84)$$

Model parameters of a one-lane traffic in the congested regime is considered and chosen, as shown in Table I.

We consider a constant incoming flow and constant outgoing density for boundary conditions

$$\tilde{q}(0,t) = 0 \quad (85)$$

$$\tilde{v}(L,t) = \frac{1}{\rho^\star}\tilde{q}(L,t). \quad (86)$$

In Section V, we validate the observer design with the traffic filed data. We do not prescribe any boundary conditions beforehand but directly take measurement of the boundary value.

We use the finite volume method, which is common in traffic flow applications. The numerical approach divides the freeway segment into cells and then approximates the cell values considering the balance of fluxes through the boundaries of the adjacent cells. In order to obtain the numerical fluxes, we write the ARZ model in the conservative variables and then apply two-stage Lax–Wendroff scheme to discretize the ARZ model in the spatiotemporal domain. The scheme is second-order accurate in space and first order in time. The spatial grid resolution is chosen to be smaller than the average vehicle size so that the numerical errors are smaller than the model errors. Therefore, the numerical simulation is valid for this continuum model.

The inhomogeneous nonlinear ARZ model written in the conservative form is given by

$$\partial_t \rho + \partial_x(\rho v) = 0 \quad (87)$$

$$\partial_t y + \partial_x(yv) = -\frac{y}{\tau} \quad (88)$$

where ρ and y are conservative variables and y is defined as

$$y = \rho(v - V(\rho)). \quad (89)$$

The numerical fluxes are then obtained by

$$F_\rho = y + \rho V(\rho) \quad (90)$$

$$F_y = \frac{y^2}{\rho} + yV(\rho). \quad (91)$$

The Lax–Wendroff numerical scheme is performed through two-stage update from (ρ_j^n, y_j^n) to $(\rho_j^{n+1}, y_j^{n+1})$.

At the first stage, the update law of (ρ_j^n, y_j^n) to $(\rho_{j+(1/2)}^{n+(1/2)}, y_{j+(1/2)}^{n+(1/2)})$ is given by

$$\rho_{j+\frac{1}{2}}^{n+\frac{1}{2}} = \frac{1}{2}(\rho_j^n + \rho_{j+1}^n) - \frac{\Delta t}{2\Delta x}\left((F_\rho)_{j+1}^n - (F_\rho)_j^n\right) \quad (92)$$

$$y_{j+\frac{1}{2}}^{n+\frac{1}{2}} = \frac{1}{2}(y_j^n + y_{j+1}^n) - \frac{\Delta t}{2\Delta x}\left((F_y)_{j+1}^n - (F_y)_j^n\right)$$
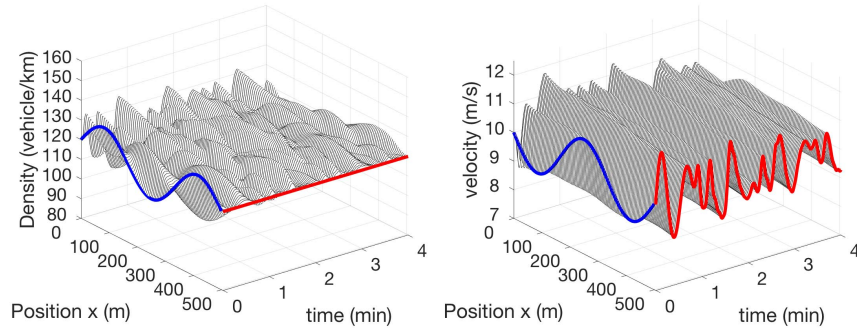$$- \frac{\Delta t}{4\tau}(y_j^n + y_{j+1}^n). \quad (93)$$

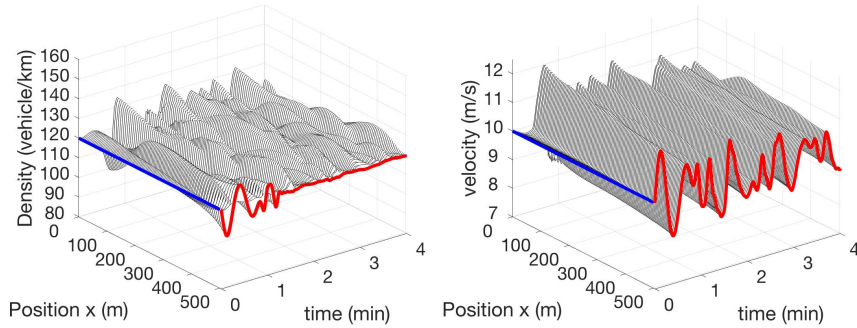Fig. 1. Density $\rho(x, t)$ and velocity $v(x, t)$ of nonlinear ARZ model.

Fig. 2. States estimates $\hat{\rho}(x, t)$ and $\hat{v}(x, t)$ of nonlinear boundary observer.
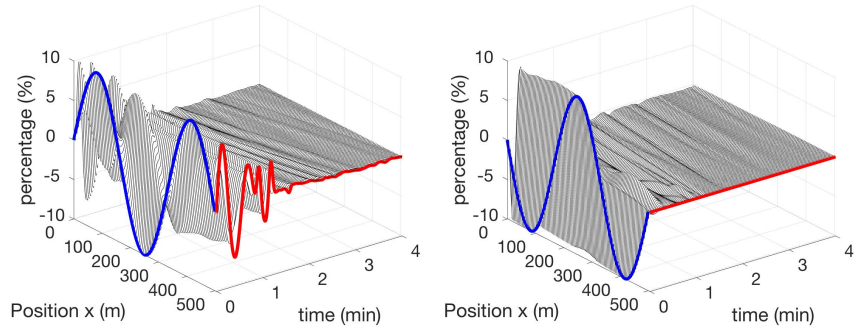

Fig. 3. Estimation errors $\check{\rho}(x, t)$ and $\check{v}(x, t)$.

Then, we calculate the numerical flux at the intermediate points of state variables and the obtained the final stage as

$$\rho_j^{n+1} = \rho_j^n - \frac{\Delta t}{\Delta x}\left(\left(F_\rho\right)_{j+\frac{1}{2}}^{n+\frac{1}{2}} - \left(F_\rho\right)_{j-\frac{1}{2}}^{n+\frac{1}{2}}\right) \tag{94}$$

$$y_j^{n+1} = y_j^n - \frac{\Delta t}{\Delta x}\left(\left(F_y\right)_{j+\frac{1}{2}}^{n+\frac{1}{2}} - \left(F_y\right)_{j-\frac{1}{2}}^{n+\frac{1}{2}}\right)$$
$$- \frac{\Delta t}{2\tau}\left(y_{j+\frac{1}{2}}^{n+\frac{1}{2}} + y_{j-\frac{1}{2}}^{n+\frac{1}{2}}\right). \tag{95}$$

For the numerical stability of the Lax–Wendroff scheme, the spatial grid size $\Delta x = 4$ m and time step $\Delta t = 0.15$ s is chosen so that the Courant-Friedrichs-Lewy (CFL) condition is satisfied

$$\max |\lambda_{1,2}| \le \frac{\Delta x}{\Delta t}. \tag{96}$$

We specify state values at both $x = 0$ and $x = L$ boundaries by implementing the boundary conditions in (85) and (86). The ARZ model picks up some combination of ρ and v at

each of the two boundaries, depending on the direction of characteristics at the boundary cells.

The numerical simulation result of the nonlinear ARZ, the nonlinear boundary observer estimation, and the estimation errors are plotted in Figs. 1–3, respectively. Blue lines represent the initial conditions, whereas the red lines represent the evolution of outlet state values in the temporal domain. The simulation is performed for a 500-m length of freeway segment and the evolution of traffic states density and velocity is plotted for 4 min.

In Fig. 1, traffic density and velocity oscillations are slightly damped. It takes the initial disturbance-generated vehicles 50 s to leave the domain, but the oscillations sustain for more than 4 min, which means that the incoming vehicles enter the acceleration–deceleration cycles under the influence of stop-and-go waves. The traffic states are in the congested regime. The stop-and-go phenomenon is demonstrated in the simulation.

State estimation of traffic density and velocity by the nonlinear implementation of the observer is shown in Fig. 2. The measurement is taken for the outgoing velocity and outgoing flow. The incoming flow is assumed to be at the set point value of the traffic flux and thus does not require measurement here. Note that in Section V, this assumption of the incoming flow is removed. The measurement of the incoming flux is used as the boundary condition of the observer to reflect its influence on the traffic state estimation of the considered segment. We do not assume any prior knowledge of the initial conditions and set the initial conditions to be at the set point density and velocity. We can see that state estimates converge to the true values after 75 s.

In Fig. 3, the evolution of estimation errors is shown. After 75 s, the state estimation errors for density and velocity converge to the value below 1% of the set point value. There are still relatively very small estimation errors remaining in the domain for two reasons. Our result only guarantees the convergence of estimates in the spatial L^2 norm. In addition, there could be nonlinearities of the error system not driven to zero by the linear output injections of the nonlinear boundary observer design.

V. Data Validation

In this section, we validate our boundary observer design with Next Generation Simulation (NGSIM) traffic data [15], which provides vehicle trajectories with substantial details and accuracy. The NGSIM trajectory data set is collected on April 13, 2005, by the Federal Highway Administration's project. The study area is a segment of Intestate 80 located at Emeryville, CA, USA. The data set gathers the trajectories of vehicles over a total of 45 minutes during rush hour: 4:00 P.M. to 4:15 P.M., 5:00 P.M. to 5:15 P.M., and 5:15 P.M. to 5:30 P.M.

First, we calibrate the nonlinear ARZ model with part of the NGSIM data to obtain the calibrated model parameters, including the steady-state values, the equilibrium velocity–density function $V(\rho)$, and the relaxation time τ. Then, the rest of the data sets are used to test the observer design for the calibrated ARZ model. The estimation results of traffic states are compared with the NGSIM data. The boundary data are extracted directly from the NGSIM data and traffic states are estimated for the considered domain. The reconstructed traffic data and boundary observer state estimates are compared.

A. Model Calibration With NGSIM Data

1) Reconstruction From Data: We aim to calibrate the ARZ model that is a macroscopic model describing aggregated values. However, the NGSIM data set consists of microscopic measurements. The data were recorded with high-speed cameras for every 0.1 s. We need to process the NGSIM trajectory data into a macroscopic scale before we can use it to calibrate the ARZ model.

The data were recorded on a 537-m-long freeway segment with six lanes for a time period of 15 min. Due to insufficient data collection at boundaries of the segment, onset and offset of recording, the viable domain we choose to use in calibration

and validation is 400 m during a time period around 10 min. When calibrating the parameters of the ARZ model and the fundamental diagram, we consider the freeway segment as a macroscopic general one-lane problem. Having being said, all six-lane state values need to be considered.

We will use Edie's formula [10] to calculate the aggregated traffic states $\rho(x, t), v(x, t)$, and $q(x, t)$ from the trajectory data of vehicles $x(t)$ with a resolution of 0.1 s. At each time instance, positions of the multiple vehicles are collected. Consider a time–space domain $[0, T] \times [0, L]$, we divide it into $N \times M$ grids

$$[i \Delta t, (i + 1)\Delta t] \times [j \Delta x, (j + 1)\Delta x]$$

where $i \in 1, 2, \ldots, N$ and $j \in 1, 2, \ldots, M$. Within each cell, we consider $\rho_{i,j}, q_{i,j}$, and $v_{i,j}$ to be constant. We use the following Edie's formula to map a set of vehicles' trajectories to speed, flow, and density over the space–time grid. For each cells, suppose that there are N_{ij} vehicle traces passing through the cell $[i \Delta t, (i + 1)\Delta t] \times [j \Delta x, (j + 1)\Delta x]$

$$\rho_{i,j} = \frac{\Sigma_{k=1}^{N_{ij}} t_k}{\Delta x \, \Delta t} \tag{97}$$

$$q_{i,j} = \frac{\Sigma_{k=1}^{N_{ij}} x_k}{\Delta x \, \Delta t} \tag{98}$$

$$v_{i,j} = \frac{q_{i,j}}{\rho_{i,j}}. \tag{99}$$

After obtaining the cell values $\rho_{i,j}, q_{i,j}$, and $v_{i,j}$, they can be later on compared with the observer estimates $\hat{\rho}_{i,j}, \hat{q}_{i,j}$, and $\hat{v}_{i,j}$ with the same griding. The number of cells is chosen such that in each cell, there is enough trajectory data. Otherwise, there could be cells that no trajectory has crossed. On the other hand, noises appear if a very fine discretization of grids is chosen. The following simulation is performed in a 41×41 grid.

We reconstruct the aggregated traffic states from all the three data sets. In Figs. 4 and 5, we show the surface plot of the density and velocity states for the data set of 4:00 P.M.–4:15 P.M. and the data set of 5:00 P.M.–5:15 P.M. The initial conditions are highlighted with the color red and the boundary conditions at the outlet are highlighted with the color blue. The congestion forms up as time goes by and propagates from the downstream to upstream. The most congested traffic appears at the inlet where the traffic density is relatively high and velocity is low.

We are mostly interested in the congested traffic where estimation of the traffic states becomes more relevant. The linearized ARZ model around the uniform reference is analyzed and employed for the observer design. By taking the average of traffic aggregated values, we obtain the reference system $\rho^\star$, $v^\star$, and $q^\star$ of each data set. Therefore, the averaged values of density, velocity, and flow in each time period are calculated and shown in Table II. We observe that among the three data set, the traffic is most congested during 5:15 P.M.–5:30 P.M. with the largest averaged density and smallest velocity value. Whether the traffic states are in the congested or free regime will be determined after we introduce the calibrated fundamental diagram.
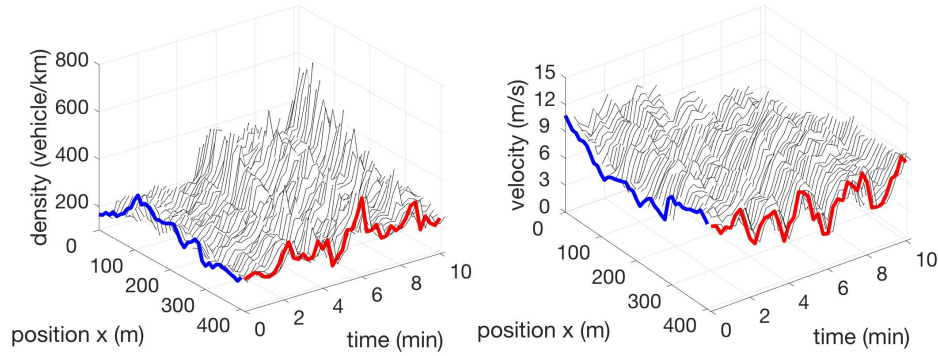
Fig. 4.   Density and velocity reconstructed from data of 4:00 P.M.–4:15 P.M.
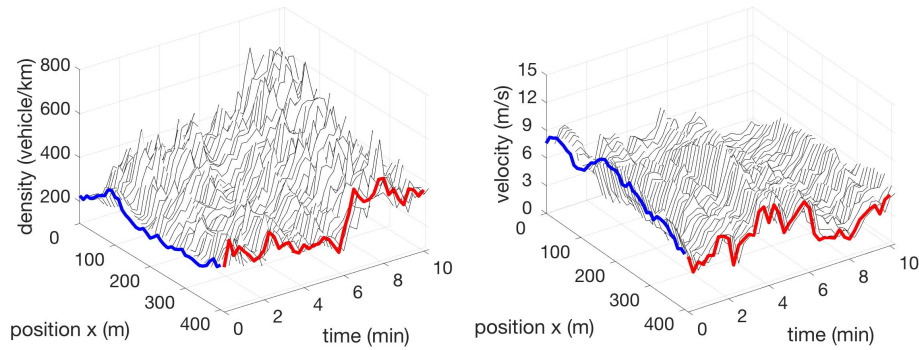

Fig. 5.   Density and velocity reconstructed from data of 5:00 P.M.–5:15 P.M.

TABLE II

AVERAGED AGGREGATE TRAFFIC DATA

Data Set	Density (veh/km)	Velocity (km/h)	Flow (veh/h)
4:00 - 4:15pm	267	28.27	7548
5:00 - 5:15pm	353	20.23	7141
5:15 - 5:30pm	375	19.35	7256

2) Calibration of Model Parameters: For the ARZ model

$$\partial_t \rho + \partial_x(\rho v) = 0 \tag{100}$$

$$\partial_t v + \big(v + \rho V'(\rho)\big)\partial_x v = \frac{V(\rho) - v}{\tau} \tag{101}$$

the model parameters to be calibrated from the data set is the equilibrium density–velocity relation $V(\rho)$ and relaxation time τ. The fundamental diagram describing the equilibrium density and flow rate relation

$$Q(\rho) = \rho V(\rho) \tag{102}$$

is usually obtained by long-term measurements via loop detectors. The loop-detector data set provides the macroscopic density and flow rate data and its recording resolution is 30 s. In Section IV, we use Greenshield's model (4) for $V(\rho)$ as a simple choice for the boundary observer design. Greenshield's fundamental diagram $Q(\rho)$ is given by

$$Q(\rho) = \rho v_f \left(1 - \left(\frac{\rho}{\rho_m}\right)^\gamma\right). \tag{103}$$

However, Greenshield's model cannot accurately represent the data for equilibrium density-flow relation. The critical density ρ_c satisfies $Q'(\rho)|_{\rho_c} = 0$ and segregates the free and congested regimes. The critical density ρ_c of Greenshield's model ($\gamma = 1$) occurs at $\rho_c = 1/2\rho_m$. However, the critical density obtained from empirical traffic data usually shows up at $\rho_c = 1/4\rho_m$. Hence, we need to consider a more realistic functional form for $Q(\rho)$. Here, we employ a three-parameter fundamental diagram proposed in [13].

In [13], the following three-parameter (λ, p, α) fundamental diagram is calibrated with the NGSIM detector data set of the same freeway segment:

$$Q(\rho) = \alpha \left(a + (b - a)\frac{\rho}{\rho_m} - \sqrt{1 + \lambda^2 \left(\frac{\rho}{\rho_m} - p\right)^2}\right) \tag{104}$$

where a and b are denoted by

$$a = \sqrt{1 + (\lambda p)^2} \tag{105}$$

$$b = \sqrt{1 + (\lambda(1 - p))^2}. \tag{106}$$

The parameters (λ, p, α) do not have physical meaning but represent the shape of the functional form where λ represents the roundness, p tunes the critical density, and α determines the maximum flow rate. The hyperbolicity $Q''(\rho) < 0$, $V'(\rho) < 0$ is guaranteed. The three parameters (λ, p, α) are determined using least-square fitting with historical loop detector data.
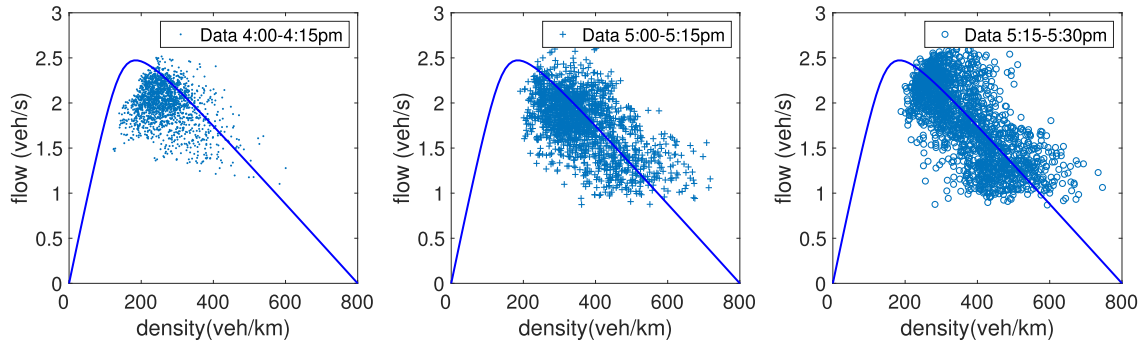
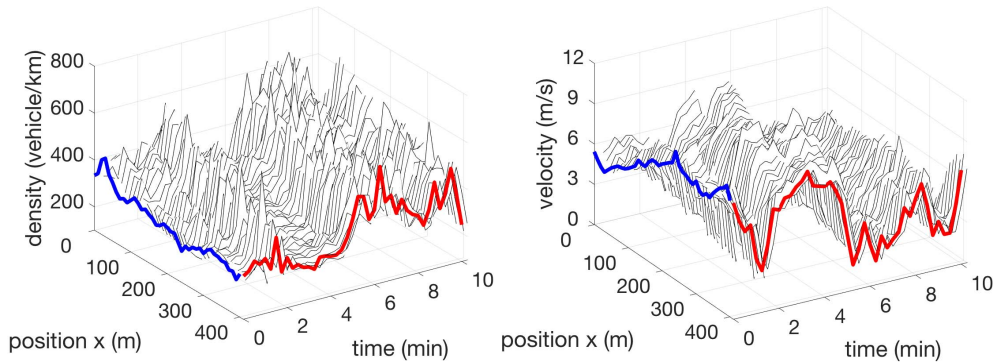Fig. 6.   Density and flow from data of 4:00 P.M.–4:15 P.M., 5:00 P.M.–5:15 P.M., and 5:15 P.M.–5:30 P.M.

Fig. 7.   Density and velocity reconstructed from the data of 5:15 P.M.–5:30 P.M.

Due to the lack of data near the maximum density, the value of ρ_m is prescribed according to the following equation:

$$\rho_m = \frac{\text{number of lanes}}{\text{typical vehicle length} \times \text{safety distance factor}}. \quad (107)$$

The freeway segment in the NGSIM data set consists of six lanes, and we consider the typical vehicle length to be 5 m and the safety distance factor is 50% of vehicle length. Therefore, we have ρ_m for all lanes in our simulation

$$\rho_m = 800 \text{ veh/km}. \quad (108)$$

The calibrated fundamental diagram is plotted in Fig. 6. The traffic density and flow rate of the three data sets are plotted on the calibrated fundamental diagram. We can see that 4:00 P.M.–4:15 P.M. are in the transition region where the data points are partially in the free regime and partially in the congested regime. The traffic data of 5:00 P.M.–5:15 P.M. and 5:15 P.M.–5:30 P.M. are scattered in the congested regime of the fundamental diagram.

With the calibrated fundamental diagram $V(\rho)$, we choose the relaxation time τ from a range from 10 to 100 s and calibrate it with the data set of 5:00 P.M.–5:15 P.M. The optimal relaxation time is $\tau = 30$ s where the total error between the calibrated model and the data is the lowest. In the next step, we use the calibrated fundamental diagram $V(\rho)$ and the relaxation time τ to construct the boundary observer.

B. Simulation for the Nonlinear Implementation of the Observer With the Calibrated Parameters

We use the data of 5:15 P.M.–5:30 P.M. to test the boundary observer design. The reference system $(\rho^\star, \upsilon^\star, q^\star)$ is obtained from Table II. Along with the calibrated parameters $V(\rho)$ and τ, the nonlinear implementation of the observer is constructed with a copy of the nonlinear ARZ model with the output injection gains that drive the estimation errors to zero. The numerical solution of the nonlinear PDEs is approximated with the Lax–Wendroff method. The boundary data are implemented with the ghost cell. The ARZ model collects the boundary values based both on the flux of the computational domain and the boundary data of the ghost cells. Using the boundary measurements of the inlet and outlet of the freeway segment, the state estimation $(\hat{\rho}(x, t), \hat{\upsilon}(x, t))$ is generated without the knowledge of the initial condition. In Fig. 7, $(\rho(x, t), \upsilon(x, t))$ is obtained from the reconstruction of the data set of 5:15 P.M.–5:30 P.M. In Fig. 8, it shows the evolution of the state estimates $(\hat{\rho}(x, t), \hat{\upsilon}(x, t))$. The initial condition, highlighted with color blue, is assumed to be the uniform reference system $(\rho^\star, \upsilon^\star, q^\star)$, which represents the averaged values of the data set. The boundary conditions at the outlet are highlighted with red color, which gives the output injections in the observer. We notice that when density values are higher than 600 veh/km at inlet around 7 min, the estimation result is not satisfying. This could be related to the ARZ model's inaccuracy in predicting traffic states near maximum density since nonunique maximum densities exist for the ARZ model, as pointed out in [14].
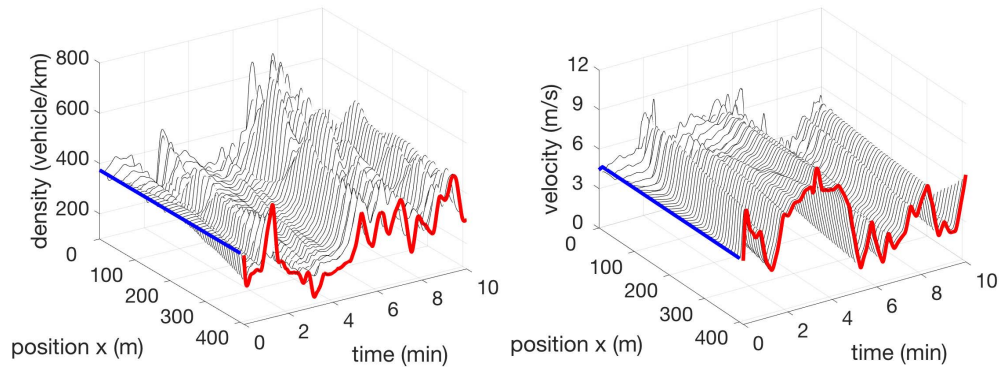
Fig. 8.　Estimates of density and velocity from the data of 5:15 P.M.–5:30 P.M.
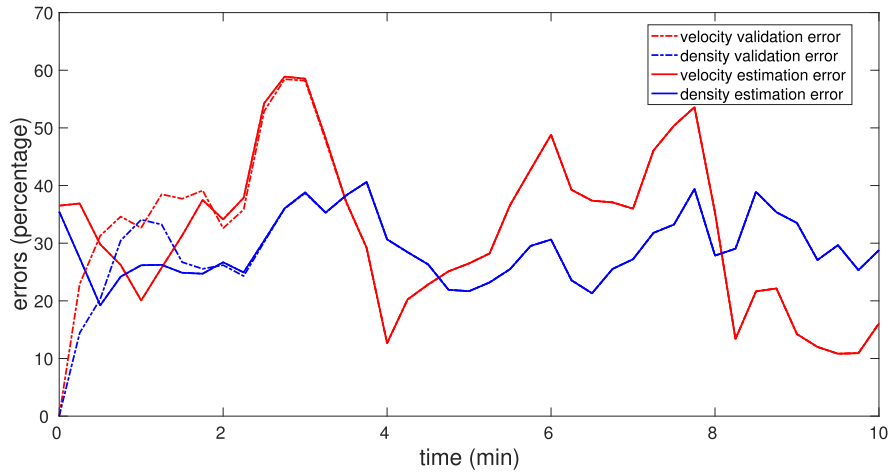

Fig. 9.　Density and velocity estimation errors and validation errors for the field data of 5:15 P.M.–5:30 P.M.

For error analysis of the observer estimation, the estimation errors are considered in the L^2-norm, defined as

$$E_\rho(t) = \left[\frac{1}{L} \int_0^L \left(\frac{\rho(x,t) - \hat{\rho}(x,t)}{\rho^\star} \right)^2 dx \right]^{1/2} \quad (109)$$

$$E_v(t) = \left[\frac{1}{L} \int_0^L \left(\frac{v(x,t) - \hat{v}(x,t)}{v^\star} \right)^2 dx \right]^{1/2} \quad (110)$$

where $\rho^\star$ and $v^\star$ are the averaged state values of the traffic data. We choose the averaged space L^2-norm of the estimation errors. The local stability in the L^2-sense for estimation errors to converge to zero is guaranteed in Theorem 2. In addition, the spatial averaged errors can remove the influence of noises and outliers of the traffic data.

The temporal evolution of the space-averaged estimation errors and validation errors of density and velocity in the L^2-sense is shown in Fig. 9. In the model validation result, the initial condition is given by the traffic field data. As can be seen in Fig. 9, the errors between the model-predicted state values and the NGSIM data, plotted with the dashed lines, are zeros at $t = 0$. The dashed lines show the evolution of the validation errors between the model-predicted values and the NGSIM data. The estimation result reveals that the errors of the density and velocity estimates start at $t = 0$ between 30% and 40%, which are also shown with the blue

lines highlighting the discrepancy between the initial condition of the data in Fig. 7 and the initial condition of the estimation states in Fig 8. The finite convergence time of the estimation values to the model-predicted values is around $t_f = 3$ min, where the dashed lines and the solid lines coincide after the convergence time.

We found out that the proposed observer accurately estimate the traffic flow states that are predicted by the ARZ PDE model. The estimation errors remaining after the convergence time are due to the model-predicted errors that come from the discrepancy between the NGSIM data and the calibrated ARZ model. The data noises, the reconstruction errors, and the numerical approximation errors could contribute to the remaining spatial averaged errors between the model-predicted values and the NGSIM traffic data.

VI. CONCLUSION

In conclusion, we develop a PDE boundary observer for the second-order nonlinear ARZ model, estimating traffic states of density and velocity, and then validate the design with the NGSIM traffic data. Analysis of the linearized ARZ model leads our main focus to the congested regime where the stop-and-go traffic appears. Using the spatial transformation and PDE backstepping method, we construct a boundary observer with a copy of the nonlinear plant and output injections

consisting of measurement errors. The exponential stability of estimation errors in the L^2 norm and finite-time convergence to zero is guaranteed. Numerical simulations are performed for a freeway segment. The nonlinear implementation of the observer is tested with a calibrated ARZ model obtained from the NGSIM data.

For future work, an observer design may be considered for a generalized ARZ model proposed in [14] to address the nonunique maximum density associated with the ARZ model. The estimation accuracy in predicting the heterogeneous behaviors of drivers and spread of data in the congested regime could be improved. On the other hand, defining the fundamental diagram requires calibration with historical data. Using the historical data to determine the model parameters could be invalid when traffic becomes unpredictable in case of sudden accidents. The limitation of the PDE backstepping observer proposed in this article is that it relies on the accuracy of the calibrated PDE model as the observer estimates the model-predicted values. It is practically preferable if the model parameters could be estimated in real time. Therefore, it is of authors' interest to consider adaptive observer design for this problem adapting the result in [34]. The robustness of the observer to uncertainty and disturbance deserves future study. The input-to-state stability to measurement errors can be proved for the proposed observer using the results in [2] and [19].

REFERENCES

[1] J. Auriol and F. Di Meglio, "Minimum time control of heterodirectional linear coupled hyperbolic PDEs," *Automatica*, vol. 71, pp. 300–307, Sep. 2016.

[2] J. Auriol and F. Di Meglio, "Robust output feedback stabilization for two heterodirectional linear coupled hyperbolic PDEs," *Automatica*, vol. 115, May 2020, Art. no. 108896.

[3] A. Aw and M. Rascle, "Resurrection of 'second order' models of traffic flow," *SIAM J. Appl. Math.*, vol. 60, no. 3, pp. 916–938, 2000.

[4] F. Belletti, M. Huo, X. Litrico, and A. M. Bayen, "Prediction of traffic convective instability with spectral analysis of the Aw–Rascle–Zhang model," *Phys. Lett. A*, vol. 379, no. 38, pp. 2319–2330, Oct. 2015.

[5] R. C. Carlson, I. Papamichail, and M. Papageorgiou, "Local feedback-based mainstream traffic flow control on motorways using variable speed limits," *IEEE Trans. Intell. Transp. Syst.*, vol. 12, no. 4, pp. 1261–1276, Dec. 2011.

[6] C. G. Claudel and A. M. Bayen, "Guaranteed bounds for traffic flow parameters estimation using mixed Lagrangian-eulerian sensing," in *Proc. 46th Annu. Allerton Conf. Commun., Control, Comput.*, Sep. 2008, p. 636.

[7] B. Coifman, "Estimating travel times and vehicle trajectories on freeways using dual loop detectors," *Transp. Res. A, Policy Pract.*, vol. 36, no. 4, pp. 351–364, May 2002.

[8] B. Coifman, "Estimating density and lane inflow on a freeway segment," *Transp. Res. A, Policy Pract.*, vol. 37, no. 8, pp. 689–701, Oct. 2003.

[9] A. Deutschmann, L. Jadachowski, and A. Kugi, "Backstepping-based boundary observer for a class of time-varying linear hyperbolic PIDEs," *Automatica*, vol. 68, pp. 369–377, Jun. 2016.

[10] L. C. Edie, "Discussion of traffic stream measurements and definitions," in *Proc. 2nd Int. Symp. Theory Road Traffic Flow*, Paris, France: Organization for Economic Co-operation and Development, 1965, p. 139–154.

[11] J.-M. Coron, R. Vazquez, M. Krstic, and G. Bastin, "Local exponential H_2 stabilization of a 2×2 quasilinear hyperbolic system using backstepping," *SIAM J. Control Optim.*, vol. 51, no. 3, pp. 2005–2035, Jan. 2013.

[12] F. Di Meglio, R. Vazquez, and M. Krstic, "Stabilization of a system of $n+1$ coupled first-order hyperbolic linear PDEs with a single boundary input," *IEEE Trans. Autom. Control*, vol. 58, no. 12, pp. 3097–3111, Dec. 2013.

[13] S. Fan and B. Seibold, "Data-fitted first-order traffic models and their second-order generalizations: Comparison by trajectory and sensor data," *Transp. Res. Record: J. Transp. Res. Board*, vol. 2391, no. 1, pp. 32–43, Jan. 2013.

[14] S. Fan, M. Herty, and B. Seibold, "Comparative model accuracy of a data-fitted generalized Aw-Rascle-Zhang model," 2013, *arXiv:1310.8219*. [Online]. Available: http://arxiv.org/abs/1310.8219

[15] FHWA, U.S. *Department of Transportation Next Generation Simulation (NGSIM)*. Accessed: Jul. 19, 2018. [Online]. Available: http://ops.fhwa.dot.gov/trafficanalysistools/ngsim.html

[16] M. R. Flynn, A. R. Kasimov, J.-C. Nave, R. R. Rosales, and B. Seibold, "Self-sustained nonlinear waves in traffic flow," *Phys. Rev. E, Stat. Phys. Plasmas Fluids Relat. Interdiscip. Top.*, vol. 79, no. 5, pp. 56–113, May 2009.

[17] D. Helbing and A. F. Johansson, "On the controversy around Daganzo's requiem for and Aw-Rascle's resurrection of second-order traffic flow models," *Eur. Phys. J. B*, vol. 69, no. 4, pp. 549–562, 2009.

[18] I. Karafyllis, N. Bekiaris-Liberis, and M. Papageorgiou, "Feedback control of nonlinear hyperbolic PDE systems inspired by traffic flow models," *IEEE Trans. Autom. Control*, vol. 64, no. 9, pp. 3647–3662, Sep. 2019.

[19] I. Karafyllis and M. Krstic, *Input-To-State Stability for PDEs*. Cham, Switzerland: Springer, 2019.

[20] I. Karafyllis and M. Papageorgiou, "Feedback control of scalar conservation laws with application to density control in freeways by means of variable speed limits," *Automatica*, vol. 105, pp. 228–236, Jul. 2019.

[21] B. S. Kerner, "Experimental features of self-organization in traffic flow," *Phys. Rev. Lett.*, vol. 81, no. 17, pp. 3797–3800, Oct. 1998.

[22] A. Kesting and M. Treiber, "Online traffic state estimation based on floating car data," 2010, *arXiv:1012.4567*. [Online]. Available: https://arxiv.org/abs/1012.4567

[23] M. J. Lighthill and G. B. Whitham, "On kinematic waves. II. A theory of traffic flow on long crowded roads," *Proc. Roy. Soc. London. Ser. A, Math. Phys. Sci.*, vol. 229, no. 1178, pp. 317–345, May 1995.

[24] L. Hu, F. Di Meglio, R. Vazquez, and M. Krstic, "Control of homodirectional and general heterodirectional linear coupled hyperbolic PDEs," *IEEE Trans. Autom. Control*, vol. 61, no. 11, pp. 3301–3314, Nov. 2016.

[25] L. Mihaylova, R. Boel, and A. Hegyi, "Freeway traffic estimation within particle filtering framework," *Automatica*, vol. 43, no. 2, pp. 290–300, Feb. 2007.

[26] M. Papageorgiou and A. Kotsialos, "Freeway ramp metering: An overview," *IEEE Trans. Intell. Transp. Syst.*, vol. 3, no. 4, pp. 271–281, Dec. 2002.

[27] H. J. Payne, "Models of freeway traffic and control," *Math. Models Public Syst.*, to be published.

[28] P. I. Richards, "Shock waves on the highway," *Oper. Res.*, vol. 4, no. 1, pp. 42–51, Feb. 1956.

[29] T. Seo, A. M. Bayen, T. Kusakabe, and Y. Asakura, "Traffic state estimation on highway: A comprehensive survey," *Annu. Rev. Control*, vol. 43, pp. 128–151, Jan. 2017.

[30] G. B. Whitham, *Linear and Nonlinear Waves*, vol. 42. Hoboken, NJ, USA: Wiley, 1974.

[31] Y. Wang and M. Papageorgiou, "Real-time freeway traffic state estimation based on extended Kalman filter: A general approach," *Transp. Res. B, Methodol.*, vol. 39, no. 2, pp. 141–167, Feb. 2005.

[32] H. Yu and M. Krstic, "Traffic congestion control for Aw-Rascle-Zhang model," *Automatica*, vol. 100, pp. 38–51, Feb. 2019.

[33] H. Yu and M. Krstic, "Varying speed limit control of Aw-Rascle-Zhang traffic model," in *Proc. 21st Int. Conf. Intell. Transp. Syst. (ITSC)*, Nov. 2018, pp. 1846–1851.

[34] H. Yu and M. Krstic, "Adaptive output feedback for Aw-Rascle-Zhang traffic model in congested regime," in *Proc. Annu. Amer. Control Conf. (ACC)*, Jun. 2018, pp. 3281–3286.

[35] H. Yu, A. M. Bayen, and M. Krstic, "Boundary observer for congested freeway traffic state estimation via Aw-Rascle-Zhang model," *IFAC-PapersOnLine*, vol. 52, no. 2, pp. 183–188, 2019.

[36] H. M. Zhang, "A non-equilibrium traffic model devoid of gas-like behavior," *Transp. Res. B, Methodol.*, vol. 36, no. 3, pp. 275–290, Mar. 2002.

[37] L. Zhang, C. Prieur, and J. Qiao, "PI boundary control of linear hyperbolic balance laws with stabilization of ARZ traffic flow models," *Syst. Control Lett.*, vol. 123, pp. 85–91, Jan. 2019.

[38] Y. Zhang and P. A. Ioannou, "Combined variable speed limit and lane change control for highway traffic," *IEEE Trans. Intell. Transp. Syst.*, vol. 18, no. 7, pp. 1812–1823, Jul. 2017.

Huan Yu received the B.S. degree in aerospace engineering from Northwestern Polytechnical University, Xi'an, China, in 2013, and the M.S. and Ph.D. degrees in mechanical and aerospace engineering from the University of California at San Diego, La Jolla, CA, USA, in 2015 and 2019, respectively.

She was a Visiting Researcher with the University of California at Berkeley, Berkeley, CA, USA, and the Massachusetts Institute of Technology, Cambridge, MA, USA. She is currently a Post-Doctoral Researcher with the University of California at San Diego. Her research focuses on the control and estimation of distributed parameter system, traffic flow control, and intelligent transportation systems.

Qijian Gan received the B.E. degree in automatic control from the University of Science and Technology of China, Hefei, China, in 2009, and the M.S. and Ph.D. degrees in civil engineering from University of California at Irvine, Irvine, CA, USA, in 2010 and 2014, respectively.

He is currently a Research and Development Engineer in the PATH Program at the University of California at Berkeley, Berkeley, CA, USA. His main expertise includes network traffic flow theory, network modeling and simulation, traffic signal control, and data analysis.

Alexandre Bayen (Member, IEEE) received the Engineering degree in applied mathematics from the École Polytechnique, Palaiseau, France, in July 1998, and the M.S. and Ph.D. degrees in aeronautics and astronautics from Stanford University, Stanford, CA, USA, in June 1999 and December 2003, respectively.

He was a Visiting Researcher with the NASA Ames Research Center, Moffett Field, CA, USA. In 2004, he was the Research Director of the Autonomous Navigation Laboratory, Laboratoire de Recherches Balistiques et Aerodynamiques (Ministere de la Defense), Vernon, France, where he holds the rank of Major. He is currently a Liao-Cho Professor of engineering, a Professor of electrical engineering and computer science, and the Director of theInstitute of Transportation Studies (ITS), the University of California at Berkeley, Berkeley, CA, USA and a Faculty Scientist in mechanical engineering at the Lawrence Berkeley National Laboratory (LBNL), Berkeley. He has authored two books and more than 200 articles in peer-reviewed journals and conferences.

Dr. Bayen has received many awards and honors, including the NSF CAREER Award, the Presidential Early Career Award for Scientists and Engineers, the IEEE Ruberti Prize, and the ASCE Huber Prize.

Miroslav Krstic (Fellow, IEEE) is currently a Distinguished Professor of mechanical and aerospace engineering, the Alspach Endowed Chair, and the Founding Director of the Cymer Center for Control Systems and Dynamics, University of California at San Diego (UCSD), La Jolla, CA, USA. He is also a Senior Associate Vice Chancellor for Research at UCSD. He has coauthored 13 books on adaptive, nonlinear, and stochastic control, extremum seeking, control of PDE systems, including turbulent flows, and control of delay systems.

Prof. Krstic has been an elected fellow of six scientific societies—IFAC, ASME, SIAM, AAAS, IET (U.K.), and AIAA (Associate Fellow)—and a Foreign Member of the Serbian Academy of Sciences and Arts and the Academy of Engineering of Serbia. He has received the SIAM Reid Prize, the ASME Oldenburger Medal, the Nyquist Lecture Prize, the Paynter Outstanding Investigator Award, the Ragazzini Education Award, the IFAC Nonlinear Control Systems Award, the Chestnut Textbook Prize, the Control Systems Society Distinguished Member Award, the PECASE, NSF Career, and ONR Young Investigator awards, the Schuck (1996 and 2019) and Axelby paper prizes, and the first UCSD Research Award given to an engineer. As a graduate student, he received the UC Santa Barbara Best Dissertation Award and student best paper awards at CDC and ACC. He received the Springer Visiting Professorship at the University of California at Berkeley, the Distinguished Visiting Fellowship of the Royal Academy of Engineering, and the Invitation Fellowship of the Japan Society for the Promotion of Science. He has served as the Vice President for Technical Activities of the IEEE Control Systems Society and the Chair for the IEEE CSS Fellow Committee. He serves as the Editor-in-Chief for *Systems & Control Letters*. He has been serving as a Senior Editor for *Automatica* and the IEEE TRANSACTIONS ON AUTOMATIC CONTROL and an Editor for two Springer book series.